

Deep learning for exploring hadron-hadron interactions

Lingxiao Wang^a

^a*Interdisciplinary Theoretical and Mathematical Sciences Program (iTHEMS), RIKEN, Wako, 351-0198, Saitama, Japan*

Abstract

In this proceeding, we introduce deep learning technologies for studying hadron-hadron interactions. To extract parameterized hadron interaction potentials from collision experiments, we employ a supervised learning approach using Femtoscopy data. The deep neural networks (DNNs) are trained to learn the inverse mapping from observations to potentials. To link between experiments and first-principles simulations, we further investigate hadronic interactions in Lattice QCD simulations from the HAL QCD method perspective. Using an unsupervised learning approach, we construct a model-free potential function with symmetric DNNs, aiming to learn hadron interactions directly from simulated correlation functions (equal-time Nambu-Bethe-Salpeter amplitudes). On both fronts, deep learning methods show great promise in advancing our understanding of hadron interactions.

Keywords: Deep Learning, Hadron Physics, Femtoscopy, Lattice QCD

1. Introduction

Hadron-hadron interactions describe the fundamental dynamics between two or more hadrons, such as protons and neutrons, or other baryons and mesons. These interactions are a manifestation of the strong interaction, which binds quarks together inside hadrons and extends to produce forces between hadrons. The earliest attempt to explain nuclear forces was made by H. Yukawa [1], proposing that the forces between nuclei are mediated by the exchange of mesons, notably the π meson, leading to the development of the Yukawa potential. Later discoveries of heavier mesons expanded it into the highly successful one-boson-exchange (OBE) framework [2, 3], which remains a cornerstone for describing interactions between hadrons.

Modern theories view hadron-hadron interactions as a residual effect of Quantum Chromodynamics (QCD), the fundamental theory of the strong interaction. Based on QCD principles, chiral effective field theory has been developed to provide a systematic framework for studying hadron-hadron interactions, incorporating QCD symmetries and allowing the study of interactions involving multiple hadrons [4, 5, 6].

First-principles calculations, such as those using lattice QCD (LQCD), have also been applied to explore hadron-hadron interactions in unprecedented detail [7, 8]. In these calculations, spatial correlations between two hadrons are analyzed to extract interaction potentials, with the HAL QCD method providing a robust tool for deriving hadron-hadron forces [9, 10, 11, 8].

On the experimental side, direct measurement of hadron interactions is not feasible. A practical and effective approach is Femtoscopy, inspired by the Hanbury Brown and Twiss (HBT) correlation [12, 13]. The Femtoscopy technique connects the correlations of particle pairs produced in high-energy collisions to hadron-hadron interactions at the femtometer scale. Advanced collision experiments, such as ALICE at

CERN-LHC and STAR at BNL-RHIC, employ Femtoscopy to measure two-body correlations and probe hadron interactions [14, 15, 16, 17]. Furthermore, this technique has been instrumental in exploring exotic hadronic states [18].

As a matter of fact, extracting hadron-hadron interaction potentials from Femtoscopy and LQCD is a typical inverse problem in QCD physics. In such problems [19], the goal is to learn the underlying physical quantity, i.e., interaction potentials, from observable data like particle correlations or equal-time Nambu-Bethe-Salpeter(NBS) amplitudes. Deep learning [20], as a modern and the most successful branch of machine learning, offers a complementary solution for inverse problems [21], with its capacity to model complex and non-linear relationships using deep neural networks (DNNs). The flexibility of deep learning frameworks enables them to generalize across diverse datasets and account for subtleties inherent in hadron-hadron systems, providing a robust tool for solving inverse problems in QCD physics.

2. Learning from Femtoscopy

2.1. Femtoscopy

Based on the femtoscopic formalism, the correlation function can be computed by convolving the source function $S(\mathbf{r})$ with the two-body scattering wave function $\psi_k(\mathbf{r})$ as follows,

$$C(k) = \int S(\mathbf{r})|\psi_k(\mathbf{r})|^2 d\mathbf{r}, \quad (1)$$

where $k = |\mathbf{p}_1 - \mathbf{p}_2|/2$ represents the relative momentum. The two-body scattering wave function, $\psi_k(\mathbf{r})$, can be determined by solving the two-body Schrödinger equation. Under the approximation of a short-range interaction potential, the wave function can be expressed in terms of the scattering length, a_0 , and the effective range of the potential, r_{eff} . In this scenario, with

a Gaussian-shaped source function, an analytical solution for $C(k)$ exists, as first developed by Lednický and Lyuboshits [22].

To achieve a more precise understanding of hadron interactions, a general framework is required for reconstructing correlation measurements. The numerical evaluation of the full wave function via the Schrödinger equation, combined with the computation of $C(k)$ for various source functions, has been implemented in two widely used tools: the Correlation Afterburner (CRAB)[23] and the ‘‘Correlation Analysis Tool using the Schrödinger equation’’ (CATS)[24, 15]. With an estimated source function [25], the correlation function $C(k)$ provides a correspondence to the interaction potential. Consequently, using numerous experimentally observed correlation functions, the hadron interaction potentials can be extracted inversely with the assistance of deep learning techniques [19].

2.2. Data Preparation

Here we employ CATS to generate training datasets. CATS provides a flexible tool to calculate correlation function $C(k)$ for different sources and interaction potentials. In this section, we utilize a parameterized form of the hadron-hadron potential and a Gaussian source. The parameters of the potential and the radius of the source are randomly sampled within reasonable ranges. Using CATS, we calculate $C(k)$ for different potentials and sources, which are then used as labelled data.

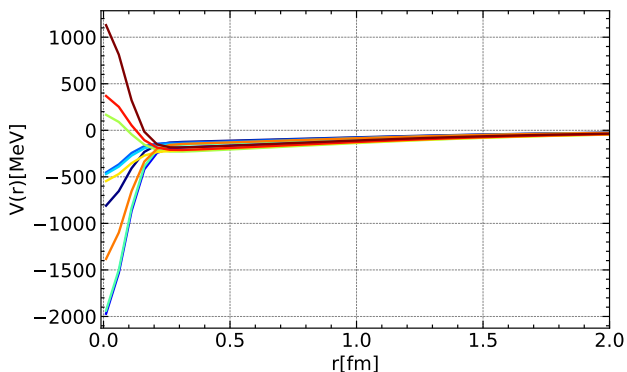


Figure 1: Hadron-hadron interaction potentials with multi-Gaussian functions as parameterizations in 10 samples.

The following parameterization is used to model the hadron interaction potential function,

$$V(r) = b_1 e^{-b_2 r^2} + b_3 (1 - e^{-b_4 r^2}) \left(\frac{e^{-m_\pi r}}{r} \right)^2, \quad (2)$$

as introduced in [26]. The parameters b_1 , b_2 , b_3 , and b_4 have physical units of MeV, fm^{-2} , $\text{MeV} \cdot \text{fm}^2$, and fm^{-2} , respectively, with the pion mass given by $m_\pi \approx 135$ MeV. For simplicity, spin-dependent interactions and other fine effects are neglected in this initial analysis. By varying the potential parameters within reasonable ranges, a variety of potentials can be generated, encompassing both repulsive and attractive interactions. The parameter ranges are as follows: b_1 varies within $[-2145.5, 1532.5]$, b_2 spans $[44.34, 103.46]$, b_3

lies within $[-345.8, -186.2]$, and b_4 ranges from $[0.702, 0.858]$. These ranges enable the exploration of diverse interaction scenarios, and 10 samples are demonstrated in Figure 1, the corresponding correlation functions can be found in Figure 2 with same colors.

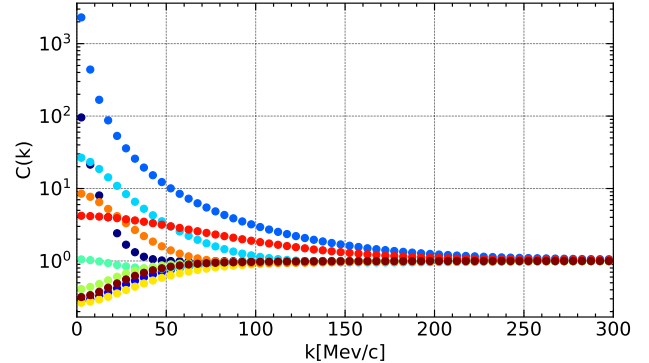


Figure 2: CATS computed correlation functions from the parameterized potential functions.

In the computation of correlation functions, we employ a Gaussian source function, where the radius r_0 serves as the controlling parameter for the source size, as described by,

$$S(r) = \frac{1}{(4\pi r_0^2)^{3/2}} \exp\left(-\frac{r^2}{4r_0^2}\right). \quad (3)$$

While determining the precise shape of source functions in different collision systems is non-trivial, we focus on the Gaussian-type source with r_0 varying in the range $[0.52, 4.16]$ fm. Notably, as shown in Ref. [25], one can construct a more accurate source function using deep neural networks when the potential functions are known.

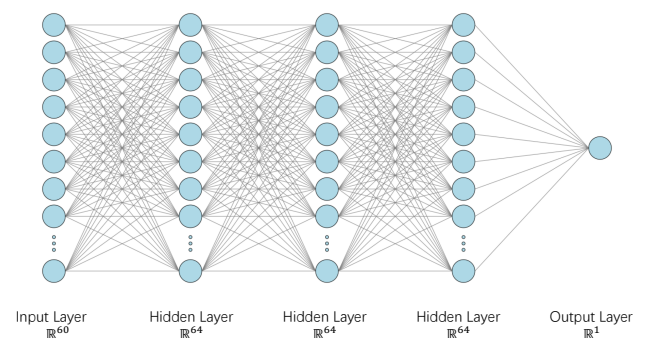


Figure 3: The deep neural network (DNN) for predicting the target parameters in potential functions from input correlation functions.

In the data preparation process, we divided the regression task into two distinct scenarios. The first scenario involves predicting one of the parameters from correlation functions computed using CATS, given 60 k -measurements uniformly distributed from 0 to 300 MeV/c. For this case, we prepared 6,400 samples for each parameter, including the source size. Unless

otherwise specified, the fixed parameter values are $r_0 = 1.3$ fm, $b_1 = -306.5$ MeV, $b_2 = 73.9$ fm⁻², $b_3 = -266$ MeV · fm², and $b_4 = 0.78$ fm⁻². The parameter being predicted is uniformly sampled from the ranges described earlier. In the second scenario, we aim to predict b_1 and b_3 simultaneously, using 10,000 samples. The remaining setup is identical to the first scenario. These two parameters were selected because they are relatively more influential in determining the shape of the potential functions. In both scenarios, the dataset is split into training and testing sets with a ratio of 8 : 2.

2.3. Learning Inverse Mapping

We develop a deep neural network (DNN) model to learn the inverse mapping from correlation functions to the parameters of potential functions. As shown in Figure 3, the basic architecture of the DNN consists of one input layer, three hidden layers, and one output layer. The input layer contains 60 nodes, corresponding to the required size of the correlation function input. Each hidden layer consists of 64 nodes. All non-activation functions between layers are chosen as ELU [27]. The final output layer is designed to predict the target label, which, in the simplest case, corresponds to one of the potential parameters.

Table 1: R^2 metric for testing data sets

| | r_0 | b_1 | b_2 | b_3 | b_4 |
|---------|-------|-------|-------|-------|-------|
| Model-1 | 0.998 | 0.999 | 0.998 | 0.999 | 0.998 |
| Model-2 | - | 0.998 | - | 0.998 | - |

In the testing set, we use the R^2 metric to evaluate the performance of the predictions. The R^2 value, or coefficient of determination, quantifies how well the model explains the variance in the target variable. It is defined as,

$$R^2 = 1 - \frac{\sum_{i=1}^n (y_i - \hat{y}_i)^2}{\sum_{i=1}^n (y_i - \bar{y})^2}, \quad (4)$$

where y_i are the target values, \hat{y}_i are the predicted values, \bar{y} is the mean of y_i , and n is the number of data points. An R^2 value of 1 indicates perfect prediction, 0 implies that the model performs no better than predicting the mean, and negative values suggest the model performs worse than the mean prediction. In Table 1, it shows the performance of two models in two scenarios, where Model-1 successfully predicts each parameter, and Model-2 also achieves $R^2 = 0.998$ for two parameters simultaneously in the testing set.

3. Learning from LQCD

3.1. HAL QCD Method

The HAL QCD method [28, 29, 30, 31] has been proposed to build effective potentials between hadrons from their spatial correlations, the equal-time Nambu-Bethe-Salpeter (NBS) amplitude $\phi_{\mathbf{k}}(\mathbf{r})$, measured on the lattice, bridging the gap between LQCD and experimental data (see e.g. [16]). Comprehensive reviews are available in Refs. [8, 32]. In this method,

the integral kernel of the integro-differential equation for the NBS wave function is treated as a non-local potential between hadrons. The non-local potential $U(\mathbf{r}, \mathbf{r}')$ for two baryons with an equal mass m_B can be defined as [28, 29, 30],

$$(E_{\mathbf{k}} - H_0)\phi_{\mathbf{k}}(\mathbf{r}) = \int d^3 r' U(\mathbf{r}, \mathbf{r}')\phi_{\mathbf{k}}(\mathbf{r}'),$$

$$E_{\mathbf{k}} = \frac{\mathbf{k}^2}{2m}, \quad H_0 = -\frac{\nabla^2}{2m}, \quad m = \frac{m_B}{2}. \quad (5)$$

Since all the elastic scattering states are governed by the same potential $U(\mathbf{r}, \mathbf{r}')$, the time-dependent HAL QCD method [31] takes full advantage of all the NBS amplitudes below the inelastic threshold $\Delta E^* \sim \Lambda_{\text{QCD}}$ by defining so-called the R correlator as $R(t, \mathbf{r}) = \sum_n^\infty A_n \psi_n(\mathbf{r}) e^{-(\Delta W_n)t} + O(e^{-(\Delta E^*)t})$, where A_n is the overlapping factor, and $\Delta W_n = 2\sqrt{m_B^2 + \mathbf{k}_n^2} - 2m_B$ with the relative momentum \mathbf{k}_n . The contributions from the inelastic states are exponentially suppressed when $t \gg (\Delta E^*)^{-1}$. In such condition, the R correlator can be shown to satisfy following integro-differential equation [31] as follows,

$$\left\{ \frac{1}{4m_B} \frac{\partial^2}{\partial t^2} - \frac{\partial}{\partial t} - H_0 \right\} R(t, \mathbf{r}) = \int d^3 \mathbf{r}' U(\mathbf{r}, \mathbf{r}') R(t, \mathbf{r}'). \quad (6)$$

The effective central potential in the leading order approximation of the velocity expansion, $U(\mathbf{r}, \mathbf{r}') = V(r)\delta(\mathbf{r} - \mathbf{r}') + \Sigma_{n=1} V_{2n}(\mathbf{r})\nabla^{2n}(\mathbf{r} - \mathbf{r}')$, can be computed directly from,

$$V(r) = \frac{1}{R(t, \mathbf{r})} \left\{ \frac{1}{4m_B} \frac{\partial^2}{\partial t^2} - \frac{\partial}{\partial t} - H_0 \right\} R(t, \mathbf{r}). \quad (7)$$

Also, the higher-order terms of the velocity expansion V_{2n} can be obtained by combining the information of the R correlators obtained from different source operators or equivalently different weight factors A_n [10].

3.2. Neural Network Hadron Potentials

To simplify the reconstruction task without loss of generality, we begin by considering the wave function in the S-wave for systems of two identical particles. To preserve the exchange symmetry inherent in the non-local potential of such systems, we design a parameter-sharing neural network [33]. Figure 4 illustrates a schematic of the symmetric deep neural network (SDNN) used to represent the potential $U_\theta(r, r')$. The inputs to the network are (r, r') , and the output from the parameter-sharing network is $f(r)$. This output is then combined with $f(r')$ as input to the subsequent layer. The final output of the network is defined as $U_\theta(r, r') \equiv g(f(r) + f(r'))$, where $g(x)$ and $f(x)$ are two distinct neural networks, and θ denotes all the trainable parameters within the neural network.

Given the wave function $\phi_{\mathbf{k}}(r)$ and the energy $E_{\mathbf{k}}$, the potential $U_\theta(r, r')$ can be determined by minimizing the loss function as the residual of Eq. (5). Furthermore, given the correlation function $R(t, r)$, the potential $U_\theta(r, r')$ can be determined through minimizing the residual of Eq. (6).

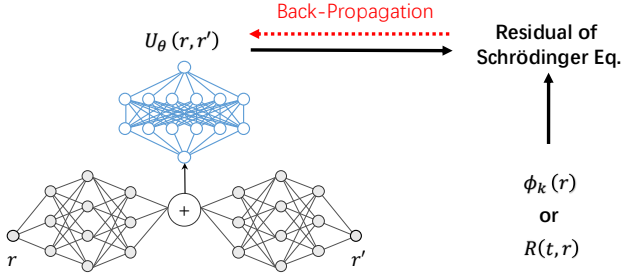


Figure 4: Symmetric deep neural network (SDNN) for representing potential functions. The gray colored neural networks are the same for inputs r and r' . The outputs of two different inputs are added in the latent layer, which is used as the input of the next layer neural network colored as blue. The final output represents $U_\theta(r, r')$.

To introduce the physical constraint as a regularization, we adopt the asymptotic behaviour of the hadron-hadron interaction, $\lim_{r, r' \rightarrow \infty} U(r, r') = 0$, as the regularization loss function,

$$\mathcal{L}_r = \sum_{n,m}^N U_\theta(r_n, r'_m)^2, \quad r_n > \tilde{R}, \quad r'_m > \tilde{R}, \quad (8)$$

where \tilde{R} is a cutoff for indicating there is zero potential. The total loss function becomes, $\mathcal{L} \equiv \mathcal{L}_{\text{data}} + \mathcal{L}_r$. As Figure 4 shows, the wave function $\phi_k(r)$ (correlation function $R(t, r)$) and potential function $U_\theta(r, r')$ are used to compute the residual, and further used to calculate the gradients to parameters of neural networks. The gradient-based algorithm, back-propagation (BP) method [34], is applied to optimize the neural network parameters $\{\theta\}$ by,

$$\theta_{i+1} \rightarrow \theta_i + \frac{\partial \mathcal{L}}{\partial U_\theta(r, r')} \frac{\partial U_\theta(r, r')}{\partial \theta}, \quad (9)$$

where the index i labels the time-step in optimization process [35, 36].

3.3. Separable Potential

We start from a solvable potential, the separable potential [8] used as a toy model for demonstration. The definition of the radial potential is,

$$U(\mathbf{r}, \mathbf{r}') \equiv \omega v(\mathbf{r})v(\mathbf{r}'), \quad v(\mathbf{r}) \equiv e^{-\mu r}, \quad (10)$$

where ω, μ are parameters. The S-wave solution of the Schrödinger equation with this potential is given exactly by,

$$\phi_k^0(r) = \frac{e^{i\delta_0(k)}}{kr} \left[\sin(kr + \delta_0(k)) - \sin \delta_0(k) e^{-\mu r} \left(1 + \frac{r(\mu^2 + k^2)}{2\mu} \right) \right]. \quad (11)$$

As a numerical example, we take $\mu = 1.0$, $\omega = -0.017\mu^4$ and $m = 3.30\mu$ and $R = 2.5/\mu$, the physics unit is chosen as μ .

When setting $\varphi_k^0(r)/r \equiv \phi_k^0(r)$, in the spherically symmetric case, the radial equation will be derived as,

$$\left(\frac{d^2}{dr^2} + k^2 \right) \varphi_k^0(r) = 8\pi m r \int r' dr' U(r, r') \varphi_k^0(r'). \quad (12)$$

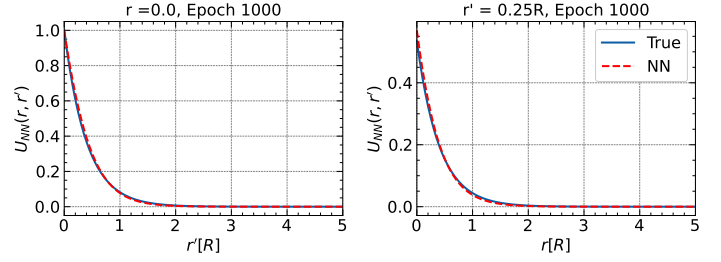


Figure 5: Reconstructed separable potentials from neural network (NN) and the ground truths.

A practical setup for preparing wave functions involves using momentum values $k = [0.01, 1.0]$ with $N_k = 10$ and radial distances $r = [0.01, 5R]$ with $N_r = 100$. A total of 1000 data points are employed to minimize the loss function for an optimal potential $U_{NN}(r, r') \equiv \omega U_\theta(r, r')$. The SDNN configuration, as illustrated in Fig. 4, consists of two identical network paths that process inputs r and r' through a series of linear transformations (structured as $1 \rightarrow 64 \rightarrow 16$) with LeakyReLU activations. These outputs are additively combined to enforce symmetry, and the merged feature is passed through a final linear layer (structured as $16 \rightarrow 1$). A Softplus activation function is applied to the output to ensure smooth, positive predictions. The reconstructed potential is shown in Fig. 5. Regularization is achieved by imposing the asymptotic behavior $U_\theta(r > \tilde{R}, r' > \tilde{R}) = 0$, where $\tilde{R} = 2R$. After 1000 epochs of training, the symmetric deep neural network successfully recovers the ground truth potential functions.

3.4. Charm Hadron Interactions

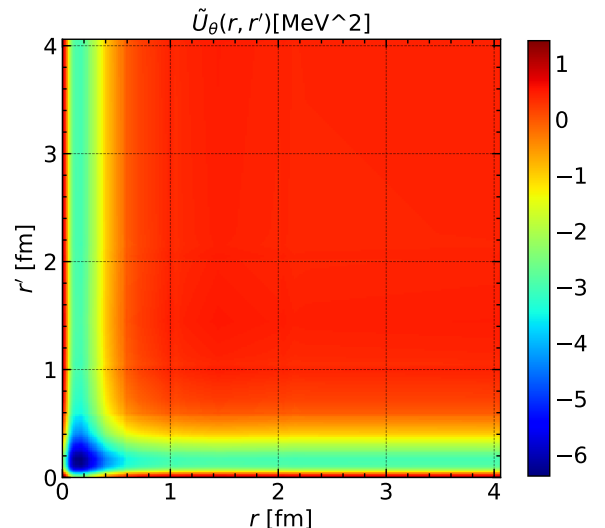


Figure 6: Non-local neural network potential for $\Omega_{ccc} - \Omega_{ccc}$.

For the second demonstration, we focus on the $\Omega_{ccc} - \Omega_{ccc}$ system, which has been extensively studied in recent research [37, 38]. The gauge configurations employed in this work utilize a $(2 + 1)$ -flavor setup on a 96^4 lattice with the

Iwasaki gauge action at $\beta = 1.82$. The lattice spacing is approximately $a \approx 0.0846$, fm ($a^{-1} \approx 2.333$, GeV), with the pion and kaon masses set to $m_\pi \approx 146$, MeV and $m_K \approx 525$, MeV, respectively. The interpolated mass of the Ω_{ccc} baryon is $m_{\Omega_{ccc}} \approx 4796$, MeV. Further details regarding the lattice setup can be found in Ref. [38].

In this setup, the symmetric deep neural network (SDNN) architecture is deeper than in the previous case, following the structure (1 \rightarrow 32 \rightarrow 64 \rightarrow 128 \rightarrow 64 \rightarrow 32 \rightarrow 16), with an ELU activation applied to the final output. Other configurations remain identical to those in the previous case. The model was trained using $R(t = 26, r)$ correlation data of the $\Omega_{ccc} - \Omega_{ccc}$ system calculated from lattice QCD simulations, where $t = 25$ and $t = 27$ were used exclusively for computing R_{tt} and R_r . Regularization was applied by enforcing the asymptotic condition $U_\theta(r > 3, \text{fm}, r' > 3, \text{fm}) = 0$. After 5000 epochs, the non-local 3D potential function, defined as $\tilde{U}_\theta(r, r') \equiv 4\pi r'^2 U_\theta(r, r')$ with $\Delta r' = 0.2a$, is demonstrated for the first time in Fig. 6.

4. Conclusions

4.1. Summary

This proceeding introduces deep learning to investigate hadron-hadron interactions. In the supervised learning approach, experimental-type Femtoscopy data are mapped to interaction potentials, while unsupervised learning, employing symmetric neural networks, derives potentials directly from Lattice QCD simulations. These methodologies demonstrate significant potential for bridging experimental observations with theoretical models, offering new insights into hadron interactions and advancing our understanding of their underlying dynamics.

4.2. Outlooks

In supervised learning, reliable simulation data sets must first be prepared, yielding physically interpretable but potentially biased results. An attempt to predict all five parameters simultaneously, however, inevitably leads to failure. In our preliminary results, this is supported by the principal component analysis (PCA) [39], which revealed that at least the first two or three components are sufficient to explain the variance in the correlation function measurements. This finding highlights the need to identify improved observables beyond correlations for extracting hadron interactions from collision experiments.

On the other hand, physics-driven designed neural networks provide a robust framework to directly extract physical quantities from observational data with greater precision. But the further comparisons between the theoretical predictions and experimental observations are still missing, in particular, we should compute the scattering phase shifts and scattering parameters more explicitly in our future works.

Acknowledgements

I would like to thank the Organizers of EMMI Workshop at the University of Wrocław - Aspects of Criticality II for the invitation to present this talk. I also thank T. Doi, T. Hatsuda,

Y. Lyu, L. Zhang and J. Zhao for discussions/material covered in my talk. I thank the members of HAL QCD Collaboration. The lattice QCD measurements have been performed on HOKUSAI supercomputers at RIKEN. This material is supported by Japan Science and Technology Agency (JST) as part of Adopting Sustainable Partnerships for Innovative Research Ecosystem (ASPIRE), Grant Number JPMJAP2318. This material is also supported by JSPS (JP19K03879, JP23H05439) and MEXT (JPMXP1020230411).

References

- [1] H. Yukawa, On the Interaction of Elementary Particles I, Proc. Phys. Math. Soc. Jap. 17 (1935) 48–57. doi:10.1143/PTPS.1.1.
- [2] R. A. Bryan, B. L. Scott, Nucleon-Nucleon Scattering from One-Boson-Exchange Potentials, Phys. Rev. 135 (1964) B434–B450. doi:10.1103/PhysRev.135.B434.
- [3] D. Kiang, M. A. Preston, P. Yip, One-boson-exchange potential and nuclear matter, Phys. Rev. 170 (1968) 907–915. doi:10.1103/PhysRev.170.907. URL <https://link.aps.org/doi/10.1103/PhysRev.170.907>
- [4] D. R. Entem, R. Machleidt, Accurate charge dependent nucleon nucleon potential at fourth order of chiral perturbation theory, Phys. Rev. C 68 (2003) 041001. arXiv:nucl-th/0304018, doi:10.1103/PhysRevC.68.041001.
- [5] R. Machleidt, D. R. Entem, Chiral effective field theory and nuclear forces, Phys. Rept. 503 (2011) 1–75. arXiv:1105.2919, doi:10.1016/j.physrep.2011.02.001.
- [6] L. Meng, B. Wang, G.-J. Wang, S.-L. Zhu, Chiral perturbation theory for heavy hadrons and chiral effective field theory for heavy hadronic molecules, Phys. Rept. 1019 (2023) 1–149. arXiv:2204.08716, doi:10.1016/j.physrep.2023.04.003.
- [7] M. L. Wagman, F. Winter, E. Chang, Z. Davoudi, W. Detmold, K. Orginos, M. J. Savage, P. E. Shanahan, Baryon-Baryon Interactions and Spin-Flavor Symmetry from Lattice Quantum Chromodynamics, Phys. Rev. D 96 (11) (2017) 114510. arXiv:1706.06550, doi:10.1103/PhysRevD.96.114510.
- [8] S. Aoki, T. Doi, Lattice QCD and baryon-baryon interactions: HAL QCD method, Front. in Phys. 8 (2020) 307. arXiv:2003.10730, doi:10.3389/fphy.2020.00307.
- [9] S. Aoki, Hadron interactions in lattice QCD, Prog. Part. Nucl. Phys. 66 (2011) 687–726. arXiv:1107.1284, doi:10.1016/j.ppnp.2011.07.001.
- [10] T. Iritani, S. Aoki, T. Doi, S. Gongyo, T. Hatsuda, Y. Ikeda, T. Inoue, N. Ishii, H. Nemura, K. Sasaki, Systematics of the HAL QCD Potential at Low Energies in Lattice QCD, Phys. Rev. D 99 (1) (2019) 014514. arXiv:1805.02365, doi:10.1103/PhysRevD.99.014514.
- [11] T. Hatsuda, Lattice quantum chromodynamics and baryon-baryon interactions, Front. Phys. (Beijing) 13 (6) (2018) 132105. doi:10.1007/s11467-018-0829-4.
- [12] S. Pratt, Pion Interferometry for Exploding Sources, Phys. Rev. Lett. 53 (1984) 1219–1221. doi:10.1103/PhysRevLett.53.1219.
- [13] M. A. Lisa, S. Pratt, R. Soltz, U. Wiedemann, Femtoscopy in relativistic heavy ion collisions, Ann. Rev. Nucl. Part. Sci. 55 (2005) 357–402. arXiv:nucl-ex/0505014, doi:10.1146/annurev.nucl.55.090704.151533.
- [14] A. Ohnishi, Hadrons, Quark-Gluon Plasma, and Neutron Stars, Springer, 2023, pp. 1–58. doi:10.1007/978-981-15-8818-1_27-1.
- [15] L. Fabbietti, V. Mantovani Sarti, O. Vazquez Doce, Study of the Strong Interaction Among Hadrons with Correlations at the LHC, Ann. Rev. Nucl. Part. Sci. 71 (2021) 377–402. arXiv:2012.09806, doi:10.1146/annurev-nucl-102419-034438.
- [16] A. Collaboration, et al., Unveiling the strong interaction among hadrons at the LHC, Nature 588 (2020) 232–238, [Erratum: Nature 590, E13 (2021)]. arXiv:2005.11495, doi:10.1038/s41586-020-3001-6.
- [17] J. Adam, et al., The Proton- Ω correlation function in Au+Au collisions at $\sqrt{s_{NN}}=200$ GeV, Phys. Lett. B 790 (2019) 490–497. arXiv:1808.02511, doi:10.1016/j.physletb.2019.01.055.

- [18] M.-Z. Liu, Y.-W. Pan, Z.-W. Liu, T.-W. Wu, J.-X. Lu, L.-S. Geng, Three ways to decipher the nature of exotic hadrons: Multiplets, three-body hadronic molecules, and correlation functions, *Phys. Rept.* 1108 (2025) 1–108. [arXiv:2404.06399](#), [doi:10.1016/j.physrep.2024.12.001](#).
- [19] K. Zhou, L. Wang, L.-G. Pang, S. Shi, Exploring QCD matter in extreme conditions with Machine Learning, *Prog. Part. Nucl. Phys.* 135 (2024) 104084. [arXiv:2303.15136](#), [doi:10.1016/j.pnpnp.2023.104084](#).
- [20] Y. LeCun, Y. Bengio, G. Hinton, Deep learning, *Nature* 521 (7553) (2015) 436–444.
- [21] A. Tanaka, A. Tomiya, K. Hashimoto, *Deep learning and physics*, Springer, 2021.
- [22] R. Lednicky, V. L. Lyuboshits, Final State Interaction Effect on Pairing Correlations Between Particles with Small Relative Momenta, *Yad. Fiz.* 35 (1981) 1316–1330.
- [23] S. Pratt, **CRAB V3.0**.
URL <https://web.pa.msu.edu/people/pratts/freecodes/crab/home.html>
- [24] D. L. Mihaylov, V. Mantovani Sarti, O. W. Arnold, L. Fabbietti, B. Hohlweger, A. M. Mathis, A femtoscopic Correlation Analysis Tool using the Schrödinger equation (CATS), *Eur. Phys. J. C* 78 (5) (2018) 394. [arXiv:1802.08481](#), [doi:10.1140/epjc/s10052-018-5859-0](#).
- [25] L. Wang, J. Zhao, Learning Hadron Emitting Sources with Deep Neural Networks (11 2024). [arXiv:2411.16343](#).
- [26] S. Aoki, T. Doi, T. Hatsuda, Y. Ikeda, T. Inoue, N. Ishii, K. Murano, H. Nemura, K. Sasaki, Lattice QCD approach to Nuclear Physics, *PTEP* 2012 (2012) 01A105. [arXiv:1206.5088](#), [doi:10.1093/ptep/pts010](#).
- [27] D.-A. Clevert, T. Unterthiner, S. Hochreiter, Fast and accurate deep network learning by exponential linear units (elus). *arXiv* 2015, *arXiv preprint arXiv:1511.07289* (2020).
- [28] N. Ishii, S. Aoki, T. Hatsuda, The Nuclear Force from Lattice QCD, *Phys. Rev. Lett.* 99 (2007) 022001. [arXiv:nucl-th/0611096](#), [doi:10.1103/PhysRevLett.99.022001](#).
- [29] S. Aoki, T. Hatsuda, N. Ishii, Nuclear Force from Monte Carlo Simulations of Lattice Quantum Chromodynamics, *Comput. Sci. Dis.* 1 (2008) 015009. [arXiv:0805.2462](#), [doi:10.1088/1749-4699/1/1/015009](#).
- [30] S. Aoki, T. Hatsuda, N. Ishii, Theoretical Foundation of the Nuclear Force in QCD and its applications to Central and Tensor Forces in Quenched Lattice QCD Simulations, *Prog. Theor. Phys.* 123 (2010) 89–128. [arXiv:0909.5585](#), [doi:10.1143/PTP.123.89](#).
- [31] N. Ishii, S. Aoki, T. Doi, T. Hatsuda, Y. Ikeda, T. Inoue, K. Murano, H. Nemura, K. Sasaki, Hadron–hadron interactions from imaginary-time Nambu–Bethe–Salpeter wave function on the lattice, *Phys. Lett. B* 712 (2012) 437–441. [arXiv:1203.3642](#), [doi:10.1016/j.physletb.2012.04.076](#).
- [32] S. Aoki, T. Doi, *Lattice QCD and Baryon-Baryon Interactions*, Springer, 2023, pp. 1–31. [arXiv:2402.11759](#), [doi:10.1007/978-981-15-8818-1_50-1](#).
- [33] L. Wang, T. Doi, T. Hatsuda, Y. Lyu, Building Hadron Potentials from Lattice QCD with Deep Neural Networks, in: *41st International Symposium on Lattice Field Theory*, 2024. [arXiv:2410.03082](#).
- [34] C. M. Bishop, H. Bishop, *Deep learning: Foundations and concepts*, Springer Nature, 2023.
- [35] L. Wang, S. Shi, K. Zhou, Reconstructing spectral functions via automatic differentiation, *Phys. Rev. D* 106 (5) (2022) L051502. [arXiv:2111.14760](#), [doi:10.1103/PhysRevD.106.L051502](#).
- [36] S. Shi, L. Wang, K. Zhou, Rethinking the ill-posedness of the spectral function reconstruction — Why is it fundamentally hard and how Artificial Neural Networks can help, *Comput. Phys. Commun.* 282 (2023) 108547. [arXiv:2201.02564](#), [doi:10.1016/j.cpc.2022.108547](#).
- [37] Y. Lyu, H. Tong, T. Sugiura, S. Aoki, T. Doi, T. Hatsuda, J. Meng, T. Miyamoto, Most charming dibaryon near unitarity, *PoS LATTICE2021* (2022) 606. [arXiv:2112.01682](#), [doi:10.22323/1.396.0606](#).
- [38] Y. Lyu, H. Tong, T. Sugiura, S. Aoki, T. Doi, T. Hatsuda, J. Meng, T. Miyamoto, Dibaryon with Highest Charm Number near Unitarity from Lattice QCD, *Phys. Rev. Lett.* 127 (7) (2021) 072003. [arXiv:2102.00181](#), [doi:10.1103/PhysRevLett.127.072003](#).
- [39] M. Greenacre, P. J. Groenen, T. Hastie, A. I. d’Enza, A. Markos, E. Tuzhilina, Principal component analysis, *Nature Reviews Methods*